Journal of Power Sources 199 (2012) 367–372

Contents lists available at SciVerse ScienceDirect

Journal of Power Sources

journal homepage: www.elsevier.com/locate/jpowsour

Characterization and optimization of a printed, primary silver–zinc battery

Kyle T. Braam[a,*], Steven K. Volkman[a], Vivek Subramanian[a,b]

[a] Department of Electrical Engineering and Computer Sciences, University of California, Berkeley, Berkeley, CA, United States
[b] World Class University Program, Sunchon National University, Suncheon, South Korea

ARTICLE INFO

Article history:
Received 3 August 2011
Received in revised form
23 September 2011
Accepted 24 September 2011
Available online 1 October 2011

Keywords:
Printed battery
Alkaline
Primary
silver–zinc
Impedance spectroscopy

ABSTRACT

The increasing deployment of ubiquitous electronic systems such as distributed sensor networks and RFID tags has resulted in a need for high energy microbatteries. Printed batteries are particularly interesting because of the potential for low material loss, low processing cost, and ease of integration into low-profile flexible electronic systems. We have developed a two-step printing technique to deposit an alkaline electrolyte for a printed silver–zinc battery. The fabricated batteries are characterized with galvanostatic measurements and electrochemical impedance spectroscopy using a three electrode setup with a zinc reference electrode. High silver utilization of $94 \pm 3\%$ and an areal energy density of 4.1 ± 0.3 mWh cm^{-2} are achieved with a 57:29:14 H_2O:KOH:PEO (M_v = 600,000) electrolyte at a $C/2$ discharge rate 1.8 mA cm^{-2}.

1. Introduction

In recent years, there has been tremendous interest in the development of a range of low-cost, ubiquitous electronic systems. For example, there has been widespread interest in the deployment of ubiquitous sensor networks [1] for such diverse applications as building monitoring [2], seismic integrity tracking [3], and product quality monitoring [4]. In addition, there has been substantial deployment of RFID systems in recent years [5,6]. Such platforms will likely necessitate the development of integrated power sources; indeed, already for active RFID and sensor network applications, there is tremendous need for small, low-cost, high energy density battery systems. Printed batteries are particularly attractive in this regard, since they will allow for easy, low-cost integration into existing and future print-based production flows. The low potential cost of fabrication and the integration ability of printed batteries are attractive for low-cost electronics, such as RFID [7], displays [8], and sensors [9,10]. As a result, in recent years, there has been widespread work on the development of technologies for the printing of batteries [11,12]. Most such printed batteries to date have been deployed using relatively low-energy density chemistries. However, printing of Li-ion microbatteries through a sol–gel process has been demonstrated with energy density of 11 μWh cm^{-2} [13]. Unfortunately, as evidenced by these relatively low areal energy-density values, even lithium-based chemistries offer poor performance with respect to areal densities in microbattery applications; this is due to the need for careful encapsulation. High specific and areal energy density batteries such as metal–air or silver–zinc batteries are desirable for these applications.

The silver–zinc battery system is particularly attractive for printing because of the high energy and areal density and air stability that this system offers, with specific energies of 200 Wh kg^{-1} and energy density of 750 Wh dm^{-3} [14]. Silver-based battery chemistries are generally not favored for typical low cost applications due to the high price of silver. However, the low-material consumption for typical printed electronic circuits makes the processing cost the dominant cost; as a result, printed silver–zinc batteries are a good candidate electrochemical system despite the relatively high cost of the silver itself. An inkjetted zinc–silver 3D battery has been demonstrated with energy density of 3.95 mWh cm^{-2} [15]. However, this system is charged by electroplating zinc from a ZnO solution and is therefore limited by the solubility of ZnO in the alkaline electrolyte.

We report the development of a primary, planar 2-dimensional printed silver zinc battery (Fig. 1). The planar architecture was chosen over a vertical structure in this paper to fabricate a fully printed battery. Printing a vertical stack for each layer (current collector, anode, electrolyte/separator, cathode, current collector) is a currently unsolved problem. A fully printed system involves developing multiple printable layers that are compatible with each other and capable of maintaining the entire weight of the cell. The planar architecture is also of interest in comparison to other planar battery systems that include microfabricated alkaline nickel–zinc

* Corresponding author at: 550 Cory Hall, University of California, Berkeley, Berkeley, CA 94704, United States. Fax: +1 510 643 4232.
E-mail address: kbraam@berkeley.edu (K.T. Braam).

0378-7753/$ – see front matter © 2011 Elsevier B.V. All rights reserved.
doi:10.1016/j.jpowsour.2011.09.076

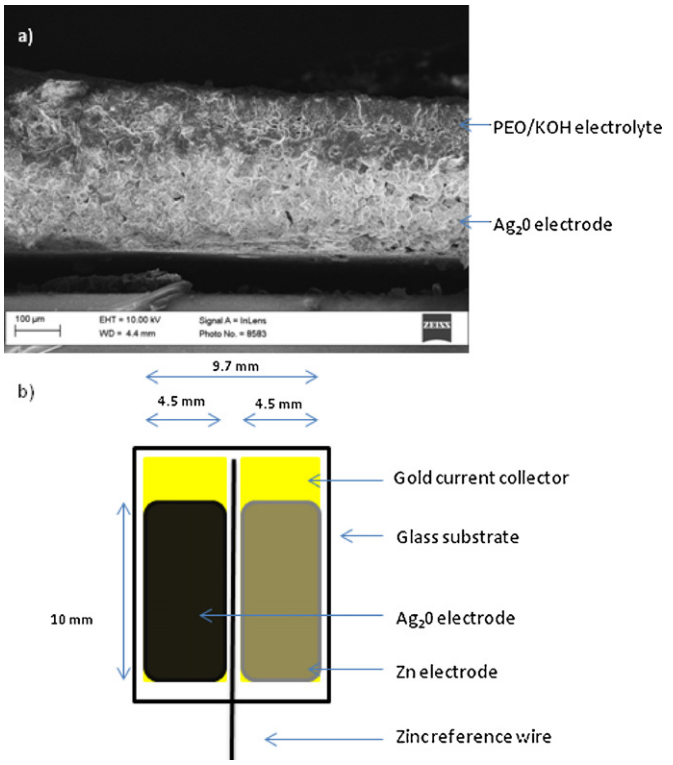

Fig. 1. a) SEM cross-section of dried discharged silver electrode and b) schematic layout of printed battery with zinc reference wire.

batteries [16], interdigitated lithium manganese oxide ($LiMn_2O_4$) and lithium titanate ($Li_{4/3}Ti_{5/3}O_4$) lithium-ion electrode microarrays [13], and laser direct-writing of Zn–AgO microbatteries [17].

To simplify our system, we examine the more stable, less alkaline soluble monovalent silver oxide (Ag_2O) instead of the higher energy density divalent form (AgO). Different molecular weights of the ionically crosslinkable polyethylene oxide (PEO) and methylcellulose are examined as a separator in an alkaline KOH electrolyte. These electrolyte layers were printed using a novel two step printing method. Galvanostatic measurements are performed to determine open circuit voltage (OCV), percent utilization and internal resistance. Electrochemical impedance spectroscopy (EIS) is used to characterize the internal equivalent circuit representations and determine the contributions of the electrolyte resistance and polarization resistance to the overall internal resistance. The chemical composition of the electrode layers before and after discharging is studied using X-ray photoelectron spectroscopy (XPS).

2. Experimental

To develop the overall printed planar battery architecture, printed anode, cathode, and electrolyte layers were developed. For the anode and cathode layers, it is necessary to develop suitable printable electrode materials. To this end, it is necessary to develop electrodes containing the active material in a binder, such that the overall formulation is suitable for printing. We first optimize the Ag_2O and Zn electrode compositions using a 50:25:25 H_2O:KOH:PEO (polyethylene oxide M_w = 12,000) electrolyte. Next the electrolyte composition is optimized with respect to polymer material (PEO and methylcellulose), polymer molecular weight, and H_2O:KOH:PEO/cellulose ratio. Polyethylene oxide is used as a separator layer due to the reported conductivities on the order of 10^{-7} S cm^{-1} [18], the ability of PEO to ionically crosslink with sodium ion in alkaline electrolyte, and the demonstration of the reduction of zinc corrosion with small molecular weight polyethylene oxide polymers [19]. Methylcellulose was used due to its use as a separator layer in alkaline battery systems [20].

Polyvinylalcohol (PVA) and polyvinylidene fluoride (PVDF) were examined as potential binding materials for the Ag_2O and Zn electrodes. Acetylene black was examined as a conductive filler to decrease the internal resistance of the electrodes and increase active material utilization. The silver oxide PVA electrode slurries were prepared by mixing with a stir bar for 1 min the appropriate amounts of silver oxide (Sigma–Aldrich) and acetylene black (50% compressed, Strem Chemicals) in aqueous solutions of 1 wt% polyvinyl alcohol (Sigma–Aldrich, M_w = 148,000–168,000). The zinc PVA electrode slurries were prepared by adding appropriate amounts of zinc (Strem Chemicals) and acetylene black to aqueous solutions of 2.5 wt% polyvinyl alcohol (Sigma–Aldrich, M_w = 148,000–168,000). Polyvinylidene fluoride (Scientific polymer, M_w = 530,000) electrode slurries were prepared by adding the appropriate amount of silver, zinc, acetylene black to 1 wt% solutions PVDF dissolved in *N*-methyl-2-pyrrolidone. Additional water or *N*-methyl-2-pyrrolidone was added if necessary to improve printing. The zinc and silver electrodes were printed using a custom built extrusion printer onto gold evaporated (60 nm) glass slides. A 2.5 nm chrome interlayer was used to improve adhesion to the glass slide. Note that evaporated contacts were used for simplicity; suitable printable routes for printing of gold contacts have been widely reported in the literature [21,22]. The separation distance between the gold current collectors was 0.7 mm, with an individual electrode area of $4.5 \times 10\,mm^2$. Silver oxide limited batteries were examined with an excess amount of Zn with a 3–4:1 Zn:Ag_2O ratio. The thickness of the silver oxide electrode was on average ~200 μm, while the zinc electrode was ~100 μm due to the differences in amount of material printed. The analysis of the zinc electrodes was performed with a ratio of 1.2–1.3:1 Ag_2O:Zn and a zinc electrode area of $2 \times 10\,mm^2$ to maintain a similar current density compared to that used in the silver oxide electrode optimization. The electrode slurries were deposited by extrusion printing followed by a drying step 40 °C. Alkaline gel electrolytes were fabricated in a two-step method. First, a polymer solution was extrusion printed on top of the electrodes, followed by pipetting the appropriate amount of potassium hydroxide from a 17 M solution solution using a micropipetter. The aqueous polymer solutions used were 50 wt% M_w = 12,000 polyethylene oxide (Sigma–Aldrich), 10 wt% M_v = 600,000 polyethylene oxide (Sigma–Aldrich), and 10 wt% methyl cellulose (27.5–32% methyl content, 10–25 mPa s at 2 wt% 20 °C). To reduce the water content of the electrolytes with 10 wt% PEO and 10 wt% methylcellulose, the batteries were partially dried to the appropriate electrolyte weight ratio at 50 °C. The final electrolyte thickness varied from 100 to 150 μm. A dried polydimethylsilicone layer was clamped on top of the batteries to improve electrode–current collector contact and prevent further drying of the battery. For an integrated cell, it is envisioned that such encapsulation could be achieved either by lamination or by direct printing of alkaline resistant polymer. One possible encapsulation scheme is lamination of the cell in polyethylene pouch [23]. The KOH was allowed to diffuse through the polymer for 30 min until a constant open circuit voltage was achieved.

Galvanostatic measurements were performed with a custom potentiostat/galvanostat [24] and a HP 4156 parameter analyzer. Electrochemical impedance spectroscopy (EIS) was carried out with a Gamry Reference 600 Potentiostat. A 3 mV RMS excitation signal was used with a frequency range of 0.1 Hz to 10^6 Hz. The EIS measurements were performed using a 3 electrode setup with a zinc reference wire between the planar electrodes. A schematic view of the battery is shown in Fig. 1.

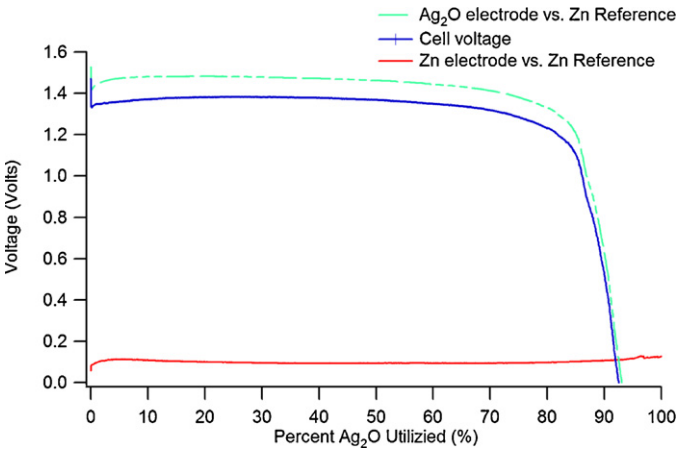

Fig. 2. A typical discharge characteristic of silver limited battery with a 50:25:25 H_2O:KOH:PEO (M_w = 12,000) electrolyte discharged at a *C*/2 rate (1.408 mA).

3. Results and discussion

3.1. Galvanostatic measurements

The Ag_2O electrode was first optimized against a 1% PVA zinc electrode in a silver limited setup by discharging at a *C*/2 rate with respect to the silver electrode with a 50:25:25 H_2O:KOH:PEO (M_w = 12,000) electrolyte. The optimum Ag_2O electrode composition was then used to optimize the zinc electrode in a zinc limited setup at a *C*/4 rate with respect to the zinc electrode. Finally, the electrolyte is analyzed with the optimized silver oxide and zinc electrodes by discharging in silver-limited cells at a *C*/2 rate.

3.2. Ag_2O electrode optimization

Two different polymers, polyvinylidene fluoride (PVDF) and polyvinyl alcohol (PVA), were examined as polymeric binder materials for both the Ag_2O and Zn electrodes. PVDF was chosen for examination since it is a hydrophobic, inert polymer and is likely to maintain electrode composition with an aqueous electrolyte. PVA was chosen for examination since it contains hydroxyl groups that can facilitate hydroxide ion transport to the electrode surface. The PVA binder provides mechanical stability by the ionic crosslinking of Na^+ ions with the hydroxyl functional group of the polymer.

Fig. 2 shows the discharge characteristic of a silver limited battery with a 50:25:25 H_2O:KOH:PEO (M_w = 12,000) electrolyte. The discharge voltage maintains a flat constant discharge voltage until 80% utilization of Ag_2O capacity. After this point, the lack of available Ag_2O and the increased resistance of the disconnected silver network results in a reduction in voltage.

High Ag_2O utilization is achieved with low percentages of PVA as a binder (Table 1). One explanation for the decreased utilization is that the PVA polymer binder is oxidized to a ketone which is caused by a reduction of Ag_2O in the presence of hydroxide ions [25]. Support for this explanation is available from the X-ray photoelectron spectra taken for PVA–5 wt% Ag_2O electrodes before and after exposure to KOH (Fig. 3). This effect results in lower Ag_2O utilization, which suggests that polyvinyl alcohol is not an optimal choice as a binder at high mass percentages. PVA would thus also not make for a good separator material in silver–zinc systems despite the reports of high hydroxide ion conductivities in PVP/PVA electrolyte [26] and PVA solid electrolytes [27]. Note that we observe that the incorporation of acetylene black does not lead to decreased internal resistance or increase Ag_2O utilization. However, the addition of acetylene black may increase the coulombic efficiency of secondary Ag–Zn batteries.

Low Ag_2O utilization was realized when PVDF was used as a polymer binder (Table 1). The low utilization is attributed to the poor mechanical stability of the polymer in the alkaline environment. PVDF is a hydrophobic polymer and unlike PVA, cannot ionically crosslink with the K^+ ions of the alkaline electrolyte. The addition of acetylene black did not improve Ag_2O utilization or decrease the internal resistance of the cell, similar to what was observed with the PVA binder.

Based on these studies, therefore, we proceed with an optimized Ag_2O electrode including 1% PVA binder, since this provides maximized silver utilization while providing good internal resistance and open circuit voltage.

3.2.1. Zn electrode optimization

The optimized silver oxide electrode with 1% PVA binder material was tested against a zinc limited cell to determine the optimal anode conditions. Similar to the silver anode, a PVA and PVDF binder with an acetylene black additive were analyzed. The 1% PVA, 2%PVA/3% acetylene black and 2% PVDF binding materials all had similar open circuit voltages and internal resistances in the zinc limited batteries (Table 2). The addition of acetylene black as a conductive filler did not have a significant effect on the zinc utilization in the current percentages added. The 1% PVA binder achieves the highest zinc utilization. However, the achieved utilization values are significantly lower than reported zinc utilizations of ~85% in 2% mercury amalgamated zinc electrodes for similar current densities [28]. The low zinc utilization observed in all three cases is likely due to a combination of loss of active material through formation of zincate species in the electrolyte in a corrosion process [29], formation of a passive ion blocking layer of ZnO and ZnOH [30], and loss of electrical contact in the porous network of zinc particles due to the formation of a ZnO/ZnOH resistive layer. The results indicate that approximately 2:1 ratio of Zn:Ag_2O is necessary for full Ag_2O utilization with the current electrode composition and current density. Reducing the amount of electrolyte will decrease the absolute quantity of zincate in the solution, which may increase the zinc utilization. The incorporation of a surfactant such as cetyltrimethylammonium bromide (CTAB) to the surface of the zinc electrode could reduce the corrosion rate of the zinc anode [31].

3.3. Electrolyte optimization

The PEO and methyl cellulose electrolyte optimizations were performed with silver limited cells, since most applications of printed batteries will necessarily work in this configuration to minimize silver cost. The electrolytes with a PEO molecular weight of M_v = 600,000 exhibited a lower internal resistance value compared

Table 1
Summary of the effect of the binder on the Ag_2O electrode with a (1:1 KOH:M_w = 12,000 PEO electrolyte) discharge at a *C*/2 cathode current of 3.7 mA cm^{-2}.

Ag_2O electrode Zn electrode	1% PVA 1% PVA	5% PVA 1% PVA	2% PVA, 3% acetylene black 1% PVA	2% PVDF 2%PVDF	2% PVDF 3% acetylene black 2% PVDF
Ag_2O utilization (%)	96 ± 3	94 ± 4	93 ± 4	80 ± 14	78 ± 11
Internal resistance (Ω)[a]	200 ± 58	227 ± 30	214 ± 37	246 ± 110	190 ± 51
Open circuit voltage (V)	1.55 ± 0.02	1.56 ± 0.02	1.55 ± 0.01	1.55 ± 0.02	1.56 ± 0.02

[a] Internal resistance is calculated as the difference in open circuit potential and discharge potential after 5 min of discharge divided by the *C*/2 current.

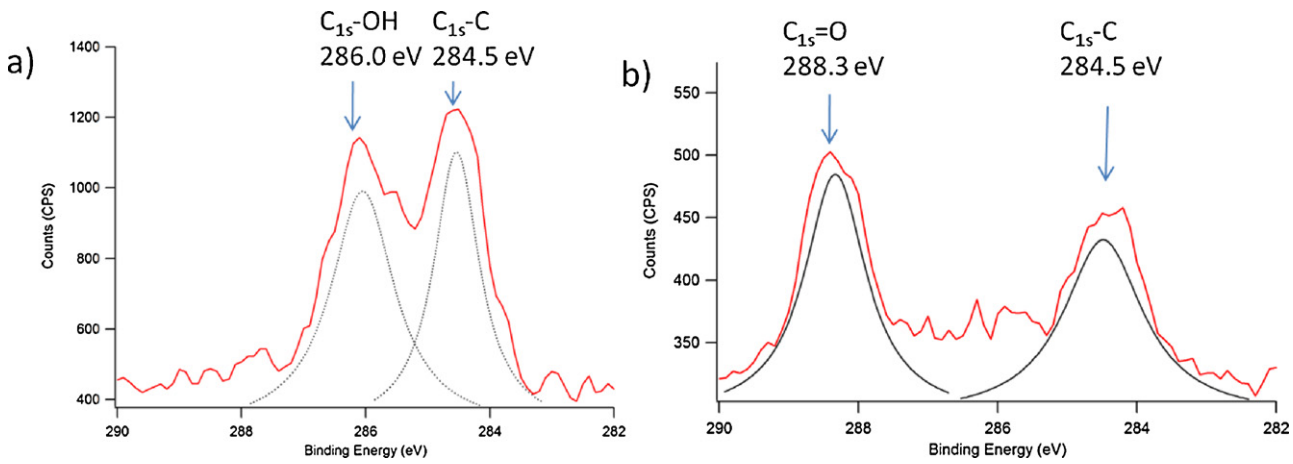

Fig. 3. a) X-ray photoelectron C1s spectrum of polyvinyl alcohol 5 wt% Ag_2O electrode. b) X-ray photoelectron C1s spectrum of polyvinyl alcohol Ag_2O electrode after placed in 1 M KOH for 5 min.

Table 2
Summary of the effect of the binder on the zinc electrode with a (1:1 KOH:M_w = 12,000 PEO electrolyte) discharged at a *C*/4 anodic current of 8.1 mA cm^{-2}.

	1% PVA	2% PVA, 3% acetylene black	2% PVDF
Zinc utilization (%)	47 ± 9	44 ± 8	38 ± 9
Internal resistance (Ω)[a]	197 ± 26	196 ± 20	210 ± 15
Open circuit voltage (V)	1.56 ± 0.04	1.56 ± 0.02	1.56 ± 0.02

[a] Internal resistance is calculated as difference in open circuit potential and discharge potential after 5 min of discharge divided by the *C*/4 discharge current.

to the PEO electrolyte with a molecular weight of M_w = 12,000 (Table 3). This is likely due to the increased portion of water in the electrolyte or due to an increase in pore size associated with high molecular weight PEO. The lower Ag_2O utilization of 66:17:17 H_2O:KOH:PEO electrolyte is attributed to the reduced hydroxide concentration and the poor hydroxide ion diffusion through the electrolyte.

Methyl cellulose as an electrolyte provided the lowest resistance of all the electrolytes examined (Table 3). However, the Ag_2O utilization is the lowest and exhibits the most variation. This low utilization to due to a shorting effect caused by the combination of the solubility of Ag_2O in KOH [25] and the ability of monovalent silver to oxidize the hydroxyl and terminal aldehyde groups of the cellulose leading to silver filaments [32]. This can be potentially reduced by using methyl cellulose with a high methyl content close to 100%. However this will reduce the solubility of cellulose in water and which would require heating to remove the excess water in low wt% solutions. The degree of polymerization of methyl cellulose can reduce the number of aldehyde groups and increase the crystallinity of the cellulose structure, but this will also lower the cellulose concentration that is printable.

The highest energy density of 58 ± 9 mWh mg^{-1} or 4.1 ± 0.3 mWh cm^{-2} was achieved with the 57:29:14 H_2O:KOH:PEO electrolyte. The energy density is comparable to the 1.2 mWh cm^{-2} achieved for a printable MnO_2–Zn ionic liquid battery [33] and an order of magnitude greater than the demonstrated 0.4 mAh cm^{-2} energy density of silicon-micromachined rechargeable nickel–zinc alkaline microbatteries [34]. The corresponding volumetric energy density is 102 mWh cm^{-3}. This volumetric energy density is comparable to that of the printed MnO_2–Zn ionic liquid battery 120 mWh cm^{-3} [15], but is slightly lower than laser direct writing of silver–zinc batteries, 400 mWh cm^{-3} [17]. In terms of commercial batteries, the as demonstrated printed Ag–Zn battery has higher volumetric energy density than that 25 mWh cm^{-3}, 1.5 V Blue Spark ST (Standard) carbon–zinc battery [35]. However, it should be noted that the commercial Blue Spark ST volumetric energy density includes packaging which reduces the overall volumetric density.

The energy density could be further improved by optimizing the zinc content to a lower ratio of Zn:Ag_2O, reducing the amount of electrolyte used, or using the higher capacity, divalent AgO instead of Ag_2O. The energy density could further be improved by reducing the internal resistance of the cell. The planar architecture chosen for this printed system is not as ideal as is a vertical structure. However, the current planar design could be improved by reducing the electrode separation distance or introducing interdigitated electrodes.

3.4. Electrochemical impedance spectroscopy (EIS)

Electrochemical impedance spectroscopy is a powerful technique to determine charge transfer kinetics, electrolyte resistance,

Table 3
Summary of electrolyte optimization for a 1% PVA Ag_2O and 1% PVA Zn electrode discharged at a *C*/2 rate.

	50:25:25 H_2O:KOH:PEO (M_w = 12,000)	57:29:14 H_2O:KOH:PEO (M_v = 600,000)	66:17:17 H_2O:KOH:PEO (M_v = 600,000)	57:29:14 H_2O:KOH:methyl cellulose
Ag_2O utilization (%)	96 ± 3	94 ± 3	78 ± 20	59 ± 32
Internal resistance (Ω)[a]	200 ± 58	135 ± 20	168 ± 18	78 ± 20
Open circuit voltage (V)	1.55 ± 0.02	1.56 ± .01	1.56 ± .01	1.56 ± 0.01
Energy density (mWh g^{-1})	49 ± 9	58 ± 9	40 ± 9	31 ± 9
Areal density (mWh cm^{-2})	4.0 ± 1	4.1 ± 0.3	2.4 ± 0.4	2.4 ± 0.6

[a] Internal resistance is calculated as difference in open circuit potential and discharge potential after 5 min of discharge divided by the *C*/2 current.

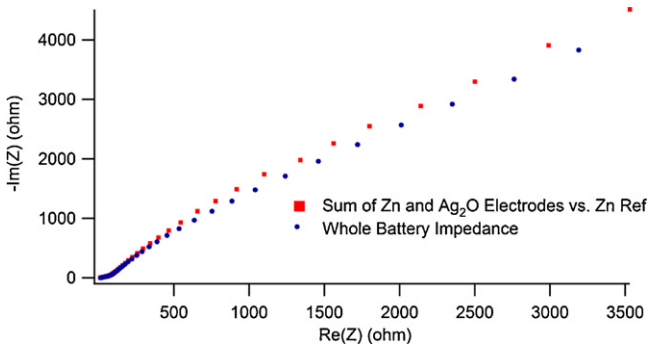

Fig. 4. Nyquist plot of 3-electrode setup with a Zn reference electrode.

and diffusion processes in electrochemical cell or at an electrode interface [36]. Here, we present an analysis of the individual electrodes of a planar, printed battery with a three-electrode setup. To analyze the performance of the full cell and half cell components, electrical impedance spectroscopy measurements were performed for the various components of the system vs. a zinc wire reference electrode. To begin, it is necessary to ensure that the zinc reference electrode indeed is suitable for use a reference electrode; i.e., it does not perturb the cell itself. Fig. 4 shows the sum of the two electrodes vs. the zinc reference electrode. The whole cell impedance is approximately equal to the sum of the individual components, $Z_{total} = Z_{zn} + Z_{Ag_2O}$, indicating the Zn reference electrode is a stable reference electrode.

The zinc electrode exhibits a two time constant impedance spectrum (Fig. 5). The electrode reaction is modeled with the equivalent circuit in the inset of Fig. 5. The high frequency component is associated with the electrochemical reaction with a charge transfer resistance, R_{ct}, and a double layer capacitance represented by a complex phase element, CPE_{dl}, with impedance:

$$Z(\omega) - \frac{1}{Q}(J\omega)^{-n}$$

The constant phase element is used instead of capacitor to take into account for distributed time constants that come from varying reactions or electrode surface inhomogenities [37]. The low frequency capacitive loop is attributed to the diffusion of the zincate into the pores of the porous electrode. The diffusion term does not exhibit the typical Warburg impedance with constant phase angle of 45°, but rather exhibits a mass transfer resistance that is attributed to the rate of diffusion not supplying the reaction quickly enough during the spectroscopic measurement [38]. The diffusion loop is modeled as the parallel combination of a polarization resistance ($Z(\omega \to \infty)$) and a complex phase element (inset, Fig. 5).

Table 4
Summary of impedance elements of Zn electrode.

$R_{electrolyte}$	R_{ct}	$Q_{CPE\text{-}DL}$	$n_{CPE\text{-}DL}$	R_P	Q_P	N_p
5.9	83.4	1.22×10^{-3}	.406	20	10.5×10^{-3}	1

The equivalent circuit parameters are summarized in Table 4. The electrolyte resistance was found to be 5.9 Ω, which is roughly half the whole cell impedance. The charge transfer resistance is 83.4 Ω. The complex phase element representing the double layer capacitance forms a depressed semicircle with an exponent value of $n = 0.403$. The diffusive loop has a complex phase element that is purely capacitive with a n value of $n = 1$. The combination of depressed semicircle followed by nearly capacitive semicircle supports the conclusion of a diffusion limited process [38]. The fact that $2R_{ct} \neq R_p$ indicates that the porous electrode does not exhibit semi-infinite pore lengths, but rather finite length pores [39].

Fig. 6 shows the impedance spectrum of the silver oxide electrode against the zinc reference electrode. The spectrum is dominated by a depressed semicircle at high frequencies that corresponds to a reduction reaction that is modeled by the parallel combination of a charge transfer resistance and double layer capacitance. At low frequencies the impedance is dominated by a Warburg diffusion term of the hydroxide ion and the oxidized species $Ag(OH)_2^-$. This species forms from the proposed mechanism of dissolution of silver oxide [36]

$$Ag_2O + 2OH^- + H_2O \leftrightarrow 2Ag(OH)_2^-$$

which is followed with the reduction of $AG(OH)_2^-$ species to silver

$$Ag(OH)_2^- + e^- \rightarrow 2(OH)^-$$

The impedance does not exhibit the traditional constant phase of 45°, but approaches a phase of 60°. Deviations from Warburg impedance have been attributed to reflective boundary conditions at the electrode [40] and to nonuniformities in polymer electrode coatings [41]. However, the deviation observed is likely due to the planar configuration of the electrodes. Finite element simulations of polymer electrolytes have shown that systems with comparable geometries (electrode length, $d = 4.5$ mm, gap, $w = 1.5$ mm, height $h = .8$ mm) have high frequency components with phases greater than 45° and are modeled with complex phase elements [42] For this reason, we model the high frequency component with a complex phase element (inset, Fig. 6). The extracted equivalent circuit

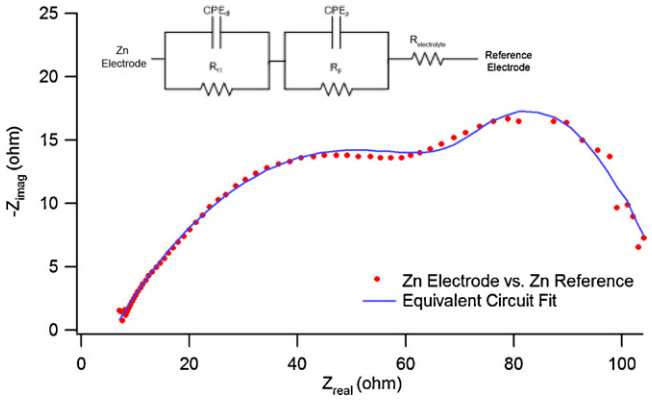

Fig. 5. Nyquist plot of the Zn electrode vs. Zn reference electrode. (inset) Equivalent circuit representation of Zn electrode vs. Zn reference wire.

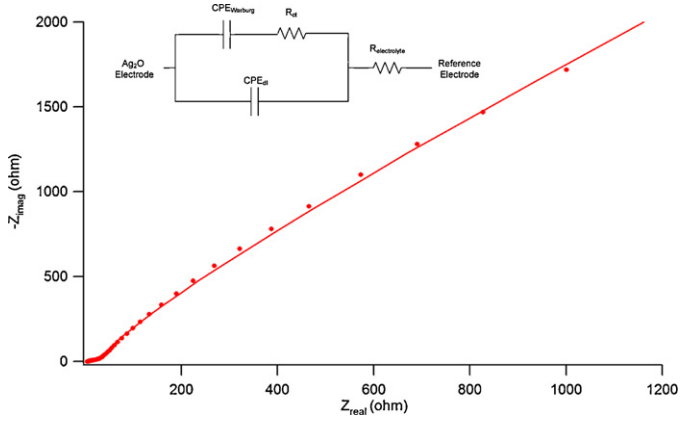

Fig. 6. Nyquist plot of the Ag_2O electrode vs. Zn reference electrode. (inset) Equivalent circuit representation of the Ag_2O electrode vs. Zn reference wire.

Table 5
Summary of impedance elements of Ag_2O electrode.

$R_{electrolyte}$ (Ω)	R_{ct}	$Q_{CPE\text{-}DL}$	$n_{CPE\text{-}Dl}$	$Q_{Warburg}$	$n_{CPE\text{-}Warburg}$
4.0	45.6	193.9×10^{-6}	.575	58.6×10^{-6}	.904

parameters of the fit are listed in Table 4. The electrolyte resistance was found to be 4 Ω, comparable to the electrolyte resistance of the zinc electrode and half of the electrolyte resistance of the whole cell. The double layer CPE has an $n = .575$, which is attributed to a rough porous electrode. The CPE of the Warburg impedance has a value of $n = .904$. This behavior is attributed to the planar nature of the electrodes (Table 5).

We therefore see that the use of EIS allows for detailed analysis of the relevant electrochemical parameters of the components of the cell. By using EIS in conjunction with a reference electrode, we have been able to isolate the dominant impedance-related phenomena in each electrode of the cell, and have thus been able to establish guidelines for further cell optimization and improvement.

4. Conclusion

The increasing deployment of ubiquitous electronic systems such as distributed sensor networks and RFID tags has resulted in a need for low cost, high energy microbatteries. In this paper we have developed a two-step printing technique to deposit an alkaline electrolyte for a printed high-energy density silver–zinc battery. An analysis of electrolytes with the polymers polyethylene oxide and methyl cellulose, found that a dried 57:29:14 H_2O:KOH:PEO ($M_v = 600{,}000$) electrolyte had the highest areal energy density of $4.1 \pm 0.3\ mWh\ cm^{-2}$ and a $94 \pm 3\%$ Ag_2O utilization at a $C/2$ discharge rate of $1.8\ mA\ cm^{-2}$. The highest Ag_2O and Zn active material utilizations were achieved with a 1% PVA binder. The half cells of the dried 57:29:14 H_2O:KOH:PEO ($M_v = 600{,}000$) electrolyte cell was further analyzed by electrochemical impedance spectroscopy in a 3 electrode setup to individual analyze each electrode. The planar electrode structure was observed in the silver oxide electrode nyquist plot and the porous nature of the zinc electrode was observed in the zinc electrode nyquist plot. The developed three electrode EIS measurement technique for a planar cell is a minimally invasive technique that can be further used examine electrode and electrolyte dependencies. The initial results for the printed battery shows promise, however further optimization of the battery design as well as the development of packaging for an alkaline cell is need for commercial applications.

Acknowledgments

Portions of this work were funded by the National Science Foundation and by the World Class University Program at Sunchon National University.

References

[1] B.A. Warneke, K.S. Pister, in: Solid-State Circuits Conference, 2004. Digest of Technical Papers. ISSCC, IEEE International 1 (2004) 316–317.
[2] S. Kim, et al., Wireless Sensor Networks for Structural Health Monitoring, 2006, p. 427.
[3] G. Werner-allen, J. Johnson, M. Ruiz, J. Lees, M. Welsh, Proceedings of the Second European Workshop on Wireless Sensor Networks (EWSN'05), 2005.
[4] J.B. Chang, et al., Journal of Applied Physics 100 (2006) 014506.
[5] S. Sarma, D. Brock, D. Engels, IEEE Micro 21 (6) (2001) 50–54.
[6] K. Finkenzeller, RFID Handbook: Fundamentals and Applications in Contactless Smart Cards and Identification, John Wiley and Sons, 2003.
[7] V. Subramanian, et al., Proceedings of the IEEE 93 (July (7)) (2005) 1330–1338.
[8] G.H. Gelinck, et al., Natural Materials 3 (February (2)) (2004) 106–110.
[9] F. Liao, C. Chen, V. Subramanian, Sensors and Actuators B: Chemical 107 (June (2)) (2005) 849–855.
[10] V. Subramanian, J.B. Lee, V.H. Liu, S. Molesa, in: Solid-State Circuits Conference, 2006. ISSCC 2006. Digest of Technical Papers, IEEE International (2006) 1052–1059.
[11] H. Lipson, et al., Freeform Fabrication of Zinc–Air Batteries and Electromechanical Assemblies.
[12] Z. Nitzan, Flexible thin layer open electrochemical cell and applications of same, U.S. Patent 589752227-Apr-1999.
[13] K. Dokko, J. -ichi Sugaya, H. Nakano, T. Yasukawa, T. Matsue, K. Kanamura, Electrochemistry Communications 9 (May (5)) (2007) 857–862.
[14] A. Karpinski, B. Makovetski, S. Russell, J. Serenyi, D. Williams, Journal of Power Sources 80 (July (1–2)) (1999) 53–60.
[15] C.C. Ho, K. Murata, D.A. Steingart, J.W. Evans, P.K. Wright, Journal of Micromechanics and Microengineering 19 (2009 September) 094013.
[16] P.H. Humble, J.N. Harb, R. LaFollette, Journal of the Electrochemical Society 148 (December (12)) (2001) A1357–A1361.
[17] A. Piqu, C.B. Arnold, H. Kim, M. Ollinger, T.E. Sutto, Applied Physics A 79 (2004 July).
[18] Y. Chun-Chen, Journal of Power Sources 109 (June (1)) (2002) 22–31.
[19] Y. Ein-Eli, Electrochemical and Solid-State Letters 7 (January (1)) (2004) B5–B7.
[20] A.N. Frumkin, E.S.B. Division, in: Proceedings of the Symposium on Rechargeable Zinc Batteries: Commemorating the 100th Birthday of A.N. Frumkin, The Electrochemical Society (1996).
[21] D. Huang, F. Liao, S. Molesa, D. Redinger, V. Subramanian, Journal of the Electrochemical Society 150 (July (7)) (2003) G412–G417.
[22] D. Redinger, et al., An Ink-Jet-Deposited Passive Component Process for RFID.
[23] A.M. Gaikwad, G.L. Whiting, D.A. Steingart, A.C. Arias, Advanced Materials 23 (August (29)) (2011) 3251–3255.
[24] D.A. Steingart, A. Redfern, C. Ho, P. Wright, J. Evans, Jonny Galvo: A Small, Low Cost Wireless Galvanostat, vol. 1, 2006, pp. 17–22.
[25] T.P. Dirkse, L.A. Vander Lugt, H. Schnyders, Journal of Inorganic and Nuclear Chemistry 25 (July (7)) (1963) 859–865.
[26] F.F. Hatta, M.Z.A. Yahya, A.M.M. Ali, R.H.Y. Subban, M.K. Harun, A.A. Mohamad, Ionics 11 (September 2005) 418–422.
[27] A. Lewandowski, K. Skorupska, J. Malinska, Solid State Ionics 133 (August (3–4)) (2000) 265–271.
[28] A. Fleischer, J.J. Lander, in: G.A. Dalin (Ed.), Zinc–Silver Oxide Batteries, J. Wiley, 1971, pp. 87–105.
[29] L. Binder, W. Odar, K. Kordesch, Journal of Power Sources 6 (December (3)) (1981) 271–289.
[30] A. Fleischer, J.J. Lander, in: N.A. Hampson (Ed.), Zinc–Silver Oxide Batteries, J. Wiley, 1971, pp. 37–61.
[31] J. Zhu, Y. Zhou, C. Gao, Journal of Power Sources 72 (April (2)) (1998) 231–235.
[32] A. Fleischer, J.J. Lander, in: P. Robert (Ed.), Zinc–Silver Oxide Batteries, J. Wiley, 1971, pp. 263–269.
[33] C.C. Ho, J.W. Evans, P.K. Wright, Journal of Micromechanics and Microengineering 20 (2010 October) 104009.
[34] F. Chamran, H.-S. Min, B. Dunn, C.-J. Kim, 19th IEEE International Conference on Micro Electro Mechanical Systems, 2006, MEMS 2006 Istanbul, 2006, pp. 950–953.
[35] "Blue_Spark_ST_Series_Batteries_09-10-1.pdf.".
[36] J.-P. Randin, Journal of Applied Electrochemistry 15 (1985 July) 591–601.
[37] G.J. Brug, A.L.G. van den Eeden, M. Sluyters-Rehbach, J.H. Sluyters, Journal of Electroanalytical Chemistry and Interfacial Electrochemistry 176 (September (1–2)) (1984) 275–295.
[38] S. Devan, V.R. Subramanian, R.E. White, Journal of the Electrochemical Society 151 (June (6)) (2004) A905–A913.
[39] M. Keddam, C. Rakotomavo, H. Takenouti, Journal of Applied Electrochemistry 14 (1984 July) 437–448.
[40] C. Criado, P. GalÃ¡n-Montenegro, P. VelÃ¡squez, J.R. Ramos-Barrado, Diffusion with general boundary conditions in electrochemical systems, Journal of Electroanalytical Chemistry 488 (June (1)) (2000) 59–63.
[41] T. Komura, S. Goisihara, T. Yamaguti, K. Takahasi, Journal of Electroanalytical Chemistry 456 (1) (1998) 121–129.
[42] A.D. Fitt, J.R. Owen, Journal of Electroanalytical Chemistry 538–539 (2002 December) 13–23.